GeoScienceWorld
Lithosphere
Volume 2022, Article ID 3824011, 14 pages
https://doi.org/10.2113/2022/3824011

Lithosphere

Research Article

Evolution of Near-Well Damage Caused by Fluid Injection through Perforations in Wellbores in Low-Permeability Reservoirs: A Case Study in a Shale Oil Reservoir

Linsheng Wang,[1] Yingyan Li,[2] Dongsheng Xu,[2] Yang Gao,[2] Jing Zhang,[2] Jixiang He,[2] Fang Zhang,[2] Sunhua Gao,[3] and Xuyang Guo [4,5]

[1]*CNPC Xinjiang Oilfield Company, 36 Yingbin Boulevard, Karamay, Xinjiang 834000, China*
[2]*Exploration and Development Research Institute of CNPC Xinjiang Oilfield Company, 29 Zhungaer Rd., Karamay, Xinjiang 834000, China*
[3]*Evinsys, 142 S Tranquil Path Dr., The Woodlands, TX 77380, USA*
[4]*College of Petroleum Engineering, China University of Petroleum (Beijing), 18 Fuxue Rd., Beijing 102249, China*
[5]*Department of Petroleum Engineering, China University of Petroleum-Beijing at Karamay, 355 Anding Rd., Karamay, Xinjiang 834000, China*

Correspondence should be addressed to Xuyang Guo; xguo@cup.edu.cn

Received 27 April 2022; Revised 28 August 2022; Accepted 30 August 2022; Published 5 October 2022

Academic Editor: Kun Xie

During the development of shale oil resources, fluid injection is usually involved in the process of hydraulic fracturing. Fluid injection through perforations causes near-well damage, which is closely related to the subsequent initiation and propagation of hydraulic fractures. This study is focused on the characterization of the temporal and spatial evolving patterns for near-well damage induced by fluid injection through perforations in the early stage of hydraulic fracturing. A coupled hydromechanical model is introduced in a case study in a shale oil reservoir in northwestern China. The model considers porous media flow during fluid injection. It also considers elasticity in the rock skeleton before the damage. Once the damage is initiated, a damage factor is employed to quantify the magnitude of injection-induced damage. Results show that damage evolution is highly sensitive to perforation number and injection rate in each individual perforation. Damage propagation is more favorable in the direction of the initial maximum horizontal principal stress. The propagation of damage is drastic at the beginning of fluid injection, while the damage front travels relatively slow afterward. This study provides insights into the near-well damage evolution before main fractures are initiated and can be used as a reference for the optimization of perforation parameters in the hydraulic fracturing design in this shale oil field.

1. Introduction

During the exploitation of hydrocarbons in low-permeability reservoirs, hydraulic fractures are usually considered as they can significantly improve the mobility of fluid flows [1]. To establish hydraulic fracture networks in low-permeability reservoirs such as shale oil reservoirs, fluids need to be injected into the reservoir to cause formation damage and eventually create artificial fractures [2–6]. Hydraulic fracturing operations are usually carried out after wellbores are drilled and completed in the reservoir, where a large volume of fluid is injected through the wellbore and through perforations to initiate damage in the formation rocks [7–11]. Since fluid injection through perforations is closely related to the near-well evolution patterns of damage, it is meaningful to quantitatively study the mechanism of how near-well damage evolves spatially and temporally under the influence of fluid injection during the exploitation of hydrocarbon resources in low-permeability reservoirs.

Reports from many sites have proved that fluid injection into deep formations associated with drilling and well completion operations can cause changes in stress and strain,

and sometimes, induced earthquakes can be observed. Hydraulic fracturing is one of these well completion techniques [12]. During the establishment of hydraulic fractures, increases in pore pressure caused by fluid injection can lead to tensile failures and shear failures in formation rocks, and these types of damage directly affect the subsequent initiation of hydraulic fractures [13–15]. Zhu et al. [16] proposed a model based on the Mohr-Coulomb criterion to quantify the coupled flow and damage behaviors during the injection process for hydraulic fracturing. Based on the flow, stress, and damage (FSD) model, they proposed that the intrinsic permeability can be increased from nano-Darcy to milli-Darcy due to the damage behaviors. Patel et al. [17] presented an experimental study of the near-well damage caused by a cyclic injection of fluids. Acoustic emission, permeability, and scanning electron microscope were used to identify the near-well damage. They indicated that the cyclic fluid injection can effectively reduce the breakdown pressure and make it easier to obtain main fractures beyond damage. Their observation proves that the prebreakdown damage evolution does have an impact on the initiation of hydraulic fracture networks. Damage theories are often combined with rock cohesions for the modeling of damage and fracture propagation during hydraulic fracturing. The injection of fluid induces normal and shear stress changes, which are used to calculate the damage factor. As the damage intensifies, damage propagation is used to represent the growth of hydraulic fractures in cohesion elements [18–20]. During the injection of fluid, stress shadows can be induced between wellbores and fractures, which makes it more difficult to achieve extensive damage propagation due to elevated compression [21, 22]. Similarly, it is also harder to obtain evenly distributed hydraulic fractures due to the stress shadows effects [23–26]. In a computational framework, Hardcastle et al. [27] computed the diffusive damage evolution in continuum space and compared the permeability changes in intact and damaged porous zones using a double permeability method. Enhanced permeability is observed in zones with induced damage. Lei et al. [28] proposed a coupled hydromechanical model to characterize the activation of fractures, the growth of damage, and the changes in connectivity caused by fluid injection in naturally fractured rocks. In their study, shearing is identified as a major consequence of fluid injection, which can be substantiated by the findings from Evans [29]. Based on the literature review, a parametric study of the effects of perforation parameters on the evolution of near-well damage is required to improve the understanding of rock damage during the pressure buildup stages in hydraulic fracturing.

In this study, a coupled hydromechanical model is presented to quantitatively analyze the injection-induced near-well damage in the initial stages of hydraulic fracturing. A numerical study is carried out to examine the effects of perforation-related parameters on the temporal and spatial evolution of damage around perforations in a shale oil case study in northwestern China. This study is focused on the damage in the pressure buildup stages and does not consider the propagation of fractures with discontinuities. This study improves the understanding of the mechanism for injection-induced damage around perforations and provides a reference for the optimization of perforation parameters for well completion in this shale oil development site.

2. Methodology

In this study, a coupled hydromechanical model is employed to characterize the injection-induced pore pressure and stress changes in a low-permeability reservoir. The coupled system solves two problems: the porous media flow problem and the geomechanical problem. It is assumed that there is single-phase flow in the porous media, and the rock skeleton exhibits elastic behaviors before damage occurs. It is also assumed that the model follows the plane strain state. For the subsurface environment, compression is treated as positive.

The fluid flow problem is described by the mass balance equation:

$$\frac{\partial}{\partial t}(\phi\rho)+\nabla\cdot(\rho v)=s, \tag{1}$$

where ρ is the fluid density; ϕ is the porosity; v is the fluid flow velocity; and s is the sink/source term.

Since the fluid flow velocity is relatively low in the porous media, Darcy's law is used to extend the fluid flow velocity term:

$$v=-\frac{k}{\mu}\cdot\nabla p, \tag{2}$$

where k is the permeability; μ is the viscosity; and p is the pore pressure. Since this study mainly considers the near-well coupled flow and geomechanics behaviors during fluid injection, strong pressure gradients are established. Therefore, it is assumed that Darcy's law can be applied in this scenario. Also, capillarity is neglected.

Since the fluid flow is slightly compressible, the compressibility of fluid is described as:

$$\chi=\frac{1}{\rho}\frac{\partial\rho}{\partial p}, \tag{3}$$

where χ is the compressibility term.

In the coupled hydromechanical model, the governing equation for the geomechanical problem is based on the momentum balance between stress components in the rock skeleton:

$$\nabla\cdot\boldsymbol{\sigma}=\boldsymbol{t}, \tag{4}$$

where $\boldsymbol{\sigma}$ is the stress tensor and $\boldsymbol{t}$ is the traction. Before damage occurs, the stress-strain constitutive relationship follows elasticity in this model. The damage near perforations is calculated based on the Mohr-Coulomb criterion for failure under compression and tension:

$$\tau=c+\sigma\tan\varphi, \tag{5}$$

where τ is the shear stress; σ is the compression; φ is the friction angle; and c is the cohesion of the rock skeleton. The criteria for tensile failure and shear failure are represented by:

$$\sigma_3 = -S_t, \tag{6}$$

$$\sigma_1 = \sigma_3 \frac{1+\sin\varphi}{1-\sin\varphi} + \frac{2c\cos\varphi}{1-\sin\varphi}, \tag{7}$$

where S_t is the tensile strength. Equation (6) is for the tensile failure criterion, and Equation (7) is for the shear failure. In Equation (6), when the injection elevates the pore pressure, compressive states in the formation can be altered to tensile states, and tensile failure may occur.

A damage parameter d is expressed as:

$$\sigma_d = (1-d)\sigma. \tag{8}$$

A loading function is used to model the damage:

$$f = \varepsilon_{eq} - \kappa, \tag{9}$$

where ε_{eq} can be expressed as $\varepsilon_{eq} = \sqrt{\varepsilon_{el} : \varepsilon_{el}}$. ε_{el} stands for elastic strain. κ is a state variable to determine the criterion for damage. The damage evolves as:

$$d = 1 - \frac{\varepsilon_0}{\kappa}\exp\left(-\frac{\kappa-\varepsilon_0}{\varepsilon_f-\varepsilon_0}\right), \kappa \geq \varepsilon_0, \tag{10}$$

$$d = 0, \kappa < \varepsilon_0. \tag{11}$$

In Equation (10) and Equation (11), $\varepsilon_0 = \sigma_t/E$, where σ_t is the tensile strength and E is the Young's modulus; $\varepsilon_f = (2G_f/\sigma_t h_{cb}) + (\varepsilon_0/2)$, where G_f is the fracture energy per unit area and h_{cb} is the element size.

3. Results and Discussion

3.1. Field Background. In this study, a model is established for the simulation of near-well damage in a shale oil-bearing formation in Jimsar Sag, Junggar Basin, in northwestern China. Target layers in the study area have low permeability, and horizontal well drilling and hydraulic fracturing techniques are widely used. The depths of payzones range from 2300 m to 4800 m. The average yearly oil production in this region is 8600 metric tons per well. Labs indicate strong brittleness for reservoir rock samples [30–32]. Since natural fractures are not prevailing in this area, they are not considered in this analysis. The stress regime is normal faulting in this region, and the range of $S_{h\,\min}$ is from 50 MPa to 75 MPa; the horizontal stress difference is between 4 MPa and 20 MPa.

3.2. Single-Perforation Base Case. A 2D model in the base case is built for the analysis of the evolution of damage near perforations. A horizontal slice crossing a perforation is the domain for the analysis. Since a plane strain state is used, a vertical stress of 75 MPa is prescribed over the domain. An initial $S_{H\,\max}$ of 65 MPa and an initial $S_{h\,\min}$ of 60 MPa are prescribed in the 2D domain.

Table 1: Input parameters for the model in the base case.

Parameters	Values
Dimension	5 m by 5 m
Perforation diameter	10 mm
Perforation number	1
Perforation location	Center of the domain
Initial pore pressure	40 MPa
Porosity	0.1
Permeability	0.1 mD
Compressibility	1×10^{-9} 1/Pa
Maximum horizontal principal stress ($S_{H\,\max}$)	65 MPa
Minimum horizontal principal stress ($S_{h\,\min}$)	60 MPa
Vertical stress	75 MPa
Elastic modulus	60 GPa
Poisson's ratio	0.25
Biot coefficient	1.0
Tensile strength	10 MPa
Fluid injection rate	0.05 kg/s
Injection time	60 s

Table 1 records the parameters used in the model. Note that since this study is focused on the evolution of near-well damage, only the early stage of fluid injection in hydraulic fracturing is studied. Figure 1 shows the setup of the numerical model with perforations around a horizontal wellbore and the 2D slice used for simulation. Since a relatively short period of time before the breakdown and propagation of hydraulic fractures is studied here, it is relatively hard to incorporate field data for validation. This is a limitation of the numerical modeling workflow.

The simulation results of the base case are then presented. Figure 2 shows the pore pressure distribution around the perforation after 1, 20, 40, and 60 seconds of constant rate injection. The constant injection rate of 0.05 kg/s can effectively elevate the near-well pore pressure. The area with elevated pore pressure increases with time. After 20 seconds, pressure is increased to more than 60 MPa near the perforation, which means that the local pore pressure is greater than the minimum principal stress and damage has occurred locally. Due to the relatively low permeability, after 60 seconds of injection, the boundary area in the domain still has relatively low pore pressure compared to near-perforation areas.

Figure 3 presents the distribution of the maximum horizontal principal stress around the perforation during fluid injection. After 1 second, $S_{H\,\max}$ changes are mainly observed in the horizontal direction near the perforation. The increase in $S_{H\,\max}$ is generally below 1 MPa, indicating that the magnitude of injection-induced stress change is limited after 1 second. However, the injection-induced stress change becomes more progressive afterward. The magnitude of $S_{H\,\max}$ largely increases in the investigated domain after

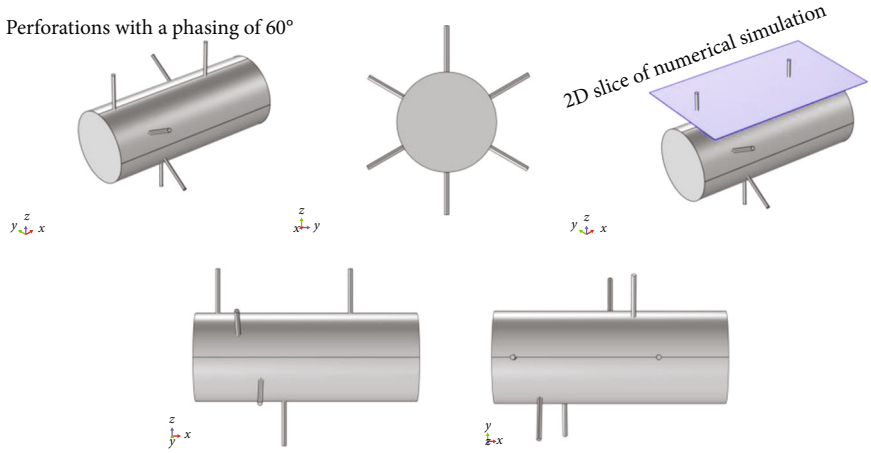

Figure 1: Perforations around a wellbore with phasing of 60° and the 2D domain used for numerical simulation.

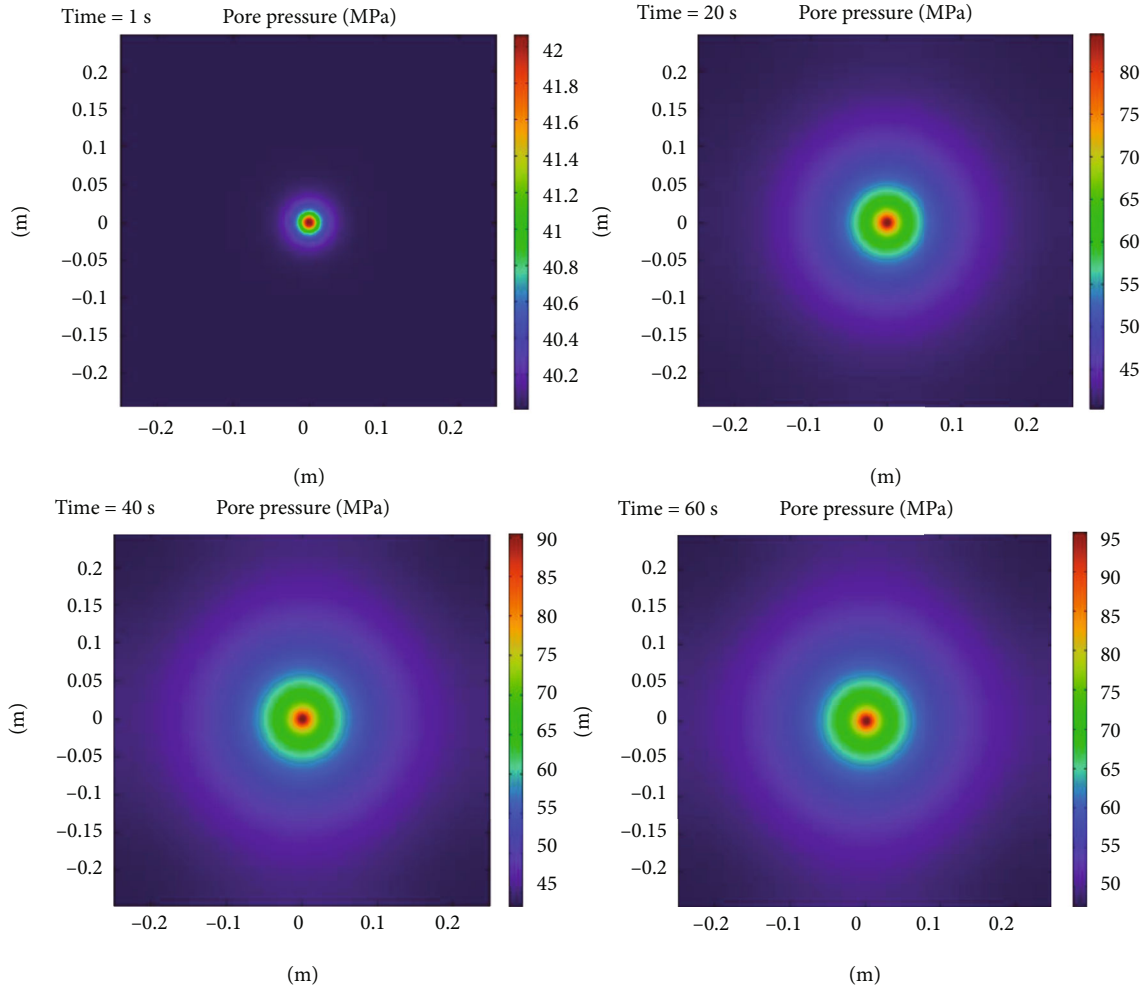

Figure 2: Elevated pore pressure around the perforation after 1, 20, 40, and 60 seconds of injection.

20, 40, and 60 seconds of constant rate injection. Another observation is that the $S_{H\ \max}$ changes in the direction of initial $S_{H\ \max}$ are greater than those in the direction of initial $S_{h\ \min}$. As the injected mass increases, the $S_{H\ \max}$ in the entire domain is largely elevated. Compared to the initial $S_{H\ \max}$ of 65 MPa, the increases in $S_{H\ \max}$ caused by the fluid injection range can reach 28 MPa around the perforation. Then, Figure 4 shows the spatial and temporal changes in the minimum horizontal principal stress. Compared to the change in $S_{H\ \max}$ in Figure 3, the change in $S_{h\ \min}$ in the vertical

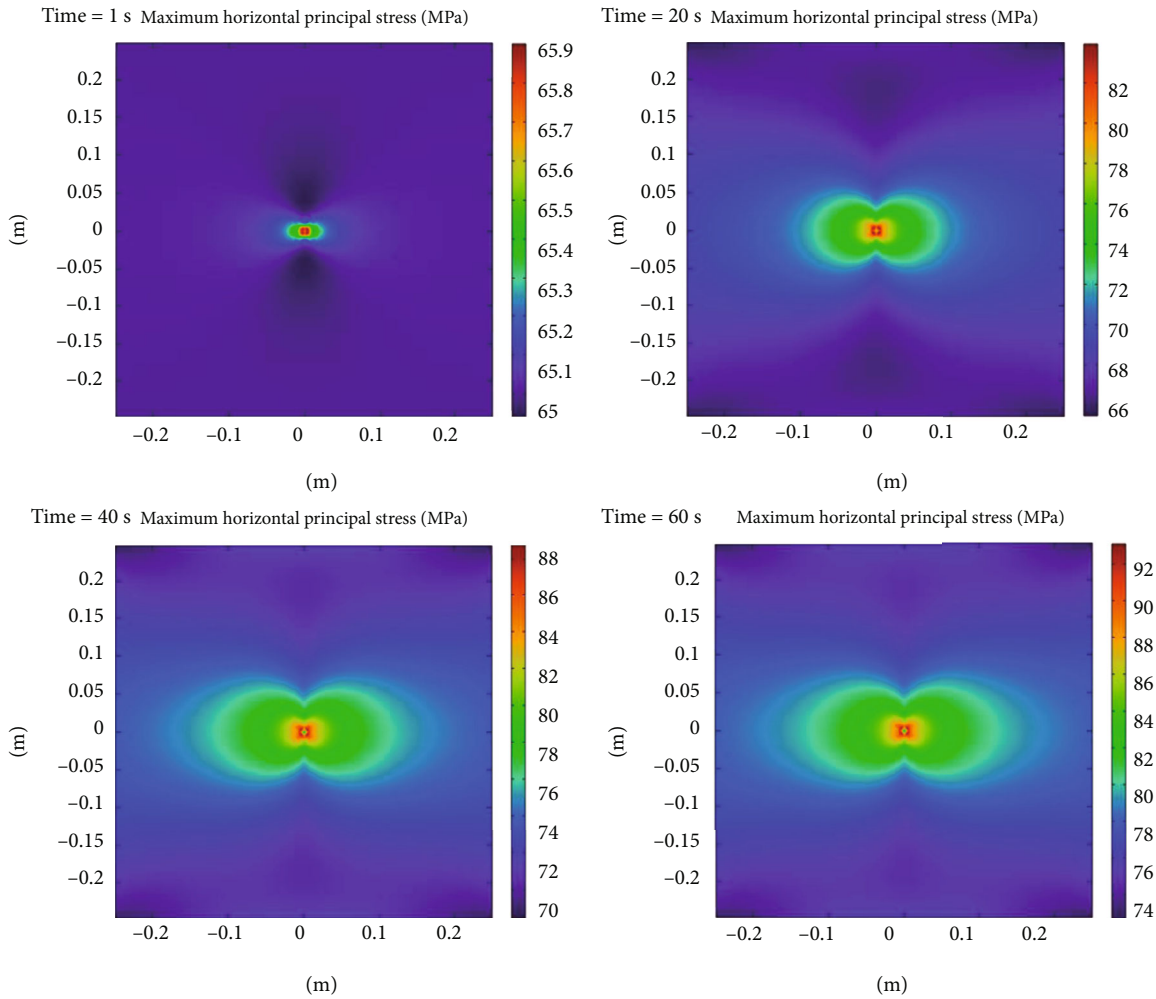

Figure 3: Maximum horizontal principal stress around the perforation after 1, 20, 40, and 60 seconds of injection.

direction is more significant. Intuitively, $S_{h\ \min}$ also increases with injection time, as the total stress consists of pore pressure and effective stress. Based on the results in Figures 2–4, injection intuitively elevates pore pressure, $S_{H\ \max}$, and $S_{h\ \min}$. However, it is noted that on time steps 20 and 40 seconds, the maximum values of $S_{H\ \max}$ and $S_{h\ \min}$ are lower than the maximum pore pressure. It indicates that the near-well areas essentially experience tension, and the original compression states are altered to tensile states, which is directly caused by fluid injection. Therefore, constant rate injection can efficiently alter the compression state to a tensile state for near-well areas.

The injection-induced damage d is plotted in Figure 5. A damage factor of zero indicates no damage while a damage factor between zero and one indicates irreversible damage to the rock skeleton. A higher damage factor always represents greater damage to the rock skeleton. Results reveal that one second of fluid injection leads to no damage within the domain. At 20 seconds, near-perforation damage can be observed, and the greatest damage is found at the perforation. Then, the magnitude and scale of the damage evolve and increase with injection time. Greater damages are observed in the direction of $S_{H\ \max}$, as the damage propagation usually aligns with the $S_{H\ \max}$ direction.

To better present the temporal change in damage and stress and pressure values, Figure 6 shows these evolutions at the perforation. Fluid injection does not instantly lead to damage at the perforation, as it needs time for pressure buildup which eventually causes irreversible damage. From around the fifth second, damage can be observed at the perforation. Afterward, the damage factor rapidly increases. After 20 seconds, the damage factor becomes more stable, and it increases to around 0.8 after 40 seconds. Based on the curves of principal stresses and pore pressure, fluid injection efficiently increases the pore pressure at the perforation. After around 10 seconds, the pore pressure becomes greater than $S_{h\ \min}$. It surpasses $S_{H\ \max}$ a few seconds later. Then, tensile stress becomes dominant in the rock skeleton in the formation at the perforation. It is also observed that drastic damage evolution is well correlated with the drastic increase in pore pressure, as pore pressure increase is the main driving force for skeleton failure. Peak values for both the maximum horizontal principal stress and the minimum horizontal principal stress are observed in the curves as well.

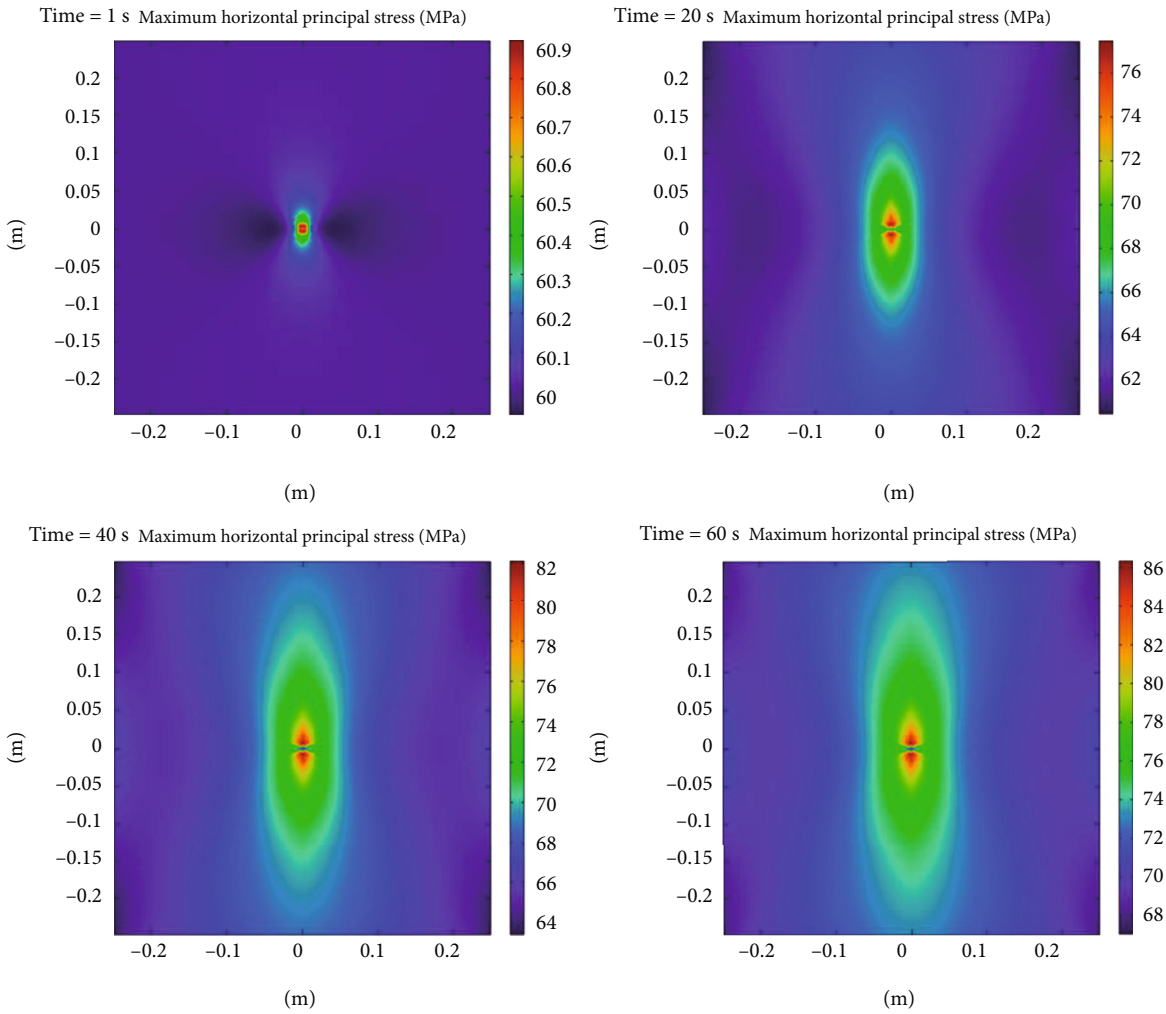

Figure 4: Minimum horizontal principal stress around the perforation after 1, 20, 40, and 60 seconds of injection.

It indicates that, although pore pressure is monotonically increasing, the compressive effective stresses (principal stresses) have maximum values. They can turn to tensile states at certain points during the fluid injection. Note that pore pressure, maximum principal horizontal stress, and minimum principal horizontal stress all monotonically increase during the late stages of fluid injection. This indicates that when the damage factor becomes stable in the late stages, the effective stresses in the rock skeleton also become relatively stable, and they are insensitive to the continued fluid injection.

The evolution of the damage factor in the x and the y directions is plotted away from the perforation. In Figure 7, the 1D spatial distribution of the damage factor in the x and in the y directions away from the perforation is plotted. The time steps presented are 1, 10, 20, 30, 40, 50, and 60 seconds. Based on the curves, sharp damage propagation fronts can be observed. Also, the damage profiles in the x direction and in the y direction are generally the same, while damage profiles in the x direction are slightly higher than those in the y direction. This means that the damage propagation is favorable in the direction of the initial maximum horizontal principal stress. This observation is in accordance with the elliptical damage profiles in Figure 5. In addition, it is observed that the damage propagation in both x and y directions is rapid at the beginning of fluid injection while it is relatively slow afterward. The damage propagates for about 5 cm in the first 10 seconds, while it takes another 50 seconds to propagate for another 5 cm later on. Therefore, the damage evolution becomes less progressive as fluid injection time increases.

3.3. Effects of Perforation Number. In the base case, the fluid injection through a single perforation and its induced near-well damage are investigated. However, during hydraulic fracturing operations, fracturing fluids are injected through multiple perforations from the wellbore. Therefore, the effect of perforation numbers is studied.

Based on the well completion data from the field, a perforation density of 16 shots/m is used, and the phasing is 60°. Since this 2D model in the study can only investigate a certain slice, based on the density and phasing data, two adjacent perforations in the same direction have a perforation spacing of 0.4 m. In this analysis, three perforation number

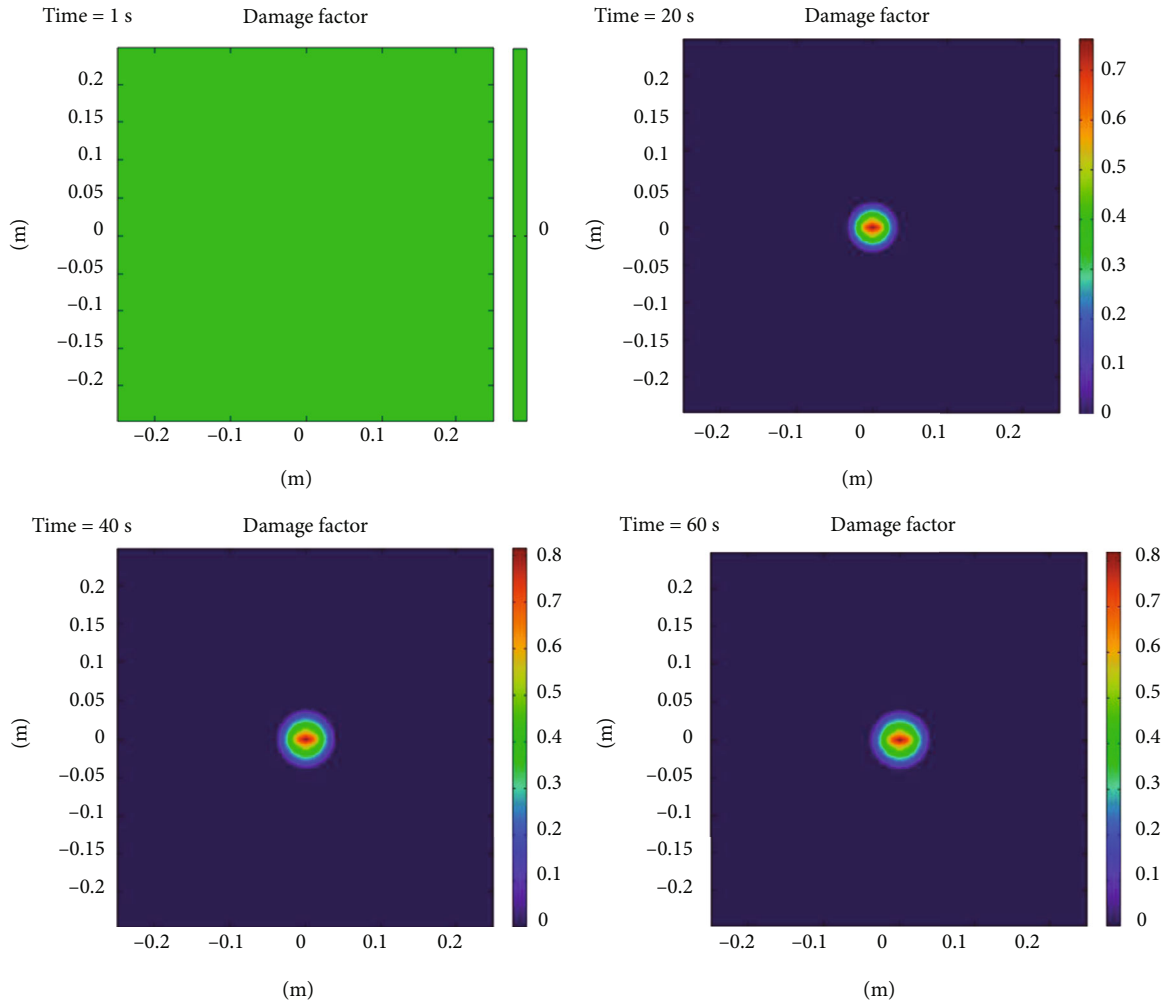

Figure 5: Damage factor around the perforation after 1, 20, 40, and 60 seconds of injection.

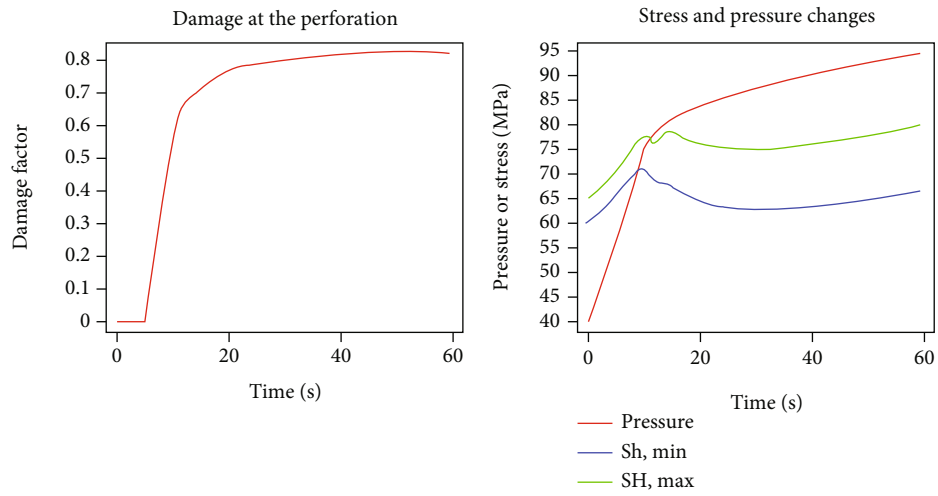

Figure 6: Damage, stress, and pressure evolutions at the perforation.

scenarios with one (base case), two, and three perforations are compared. The perforation spacing is always kept at 0.4 m when there is more than one perforation. Also, it is important to prescribe that the overall fluid injection rate is kept constant at 0.05 kg/s, and the injection rate at each perforation decreases as the perforation number increases.

The results for the near-well damage caused by fluid injection from a single perforation are already discussed in

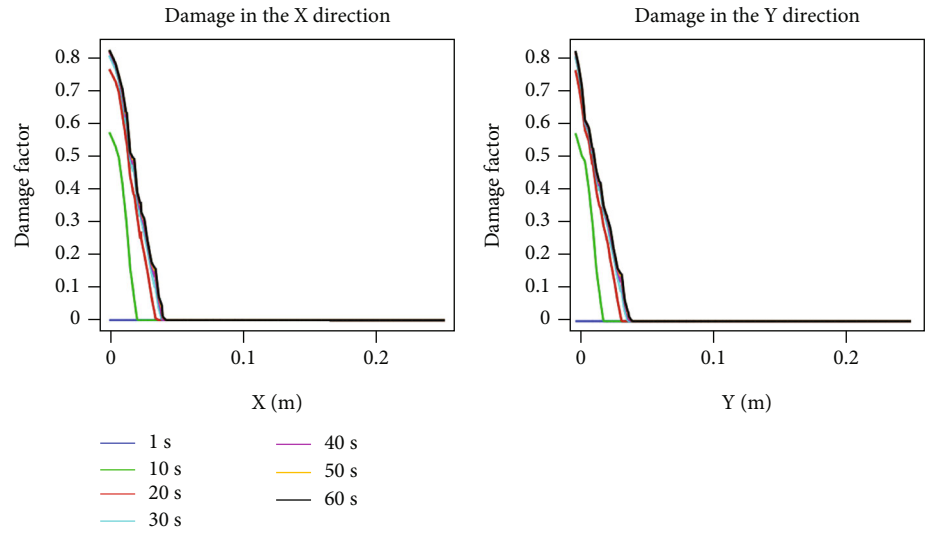

Figure 7: Damage evolutions in the x and the y directions away from the perforation at various fluid injection time steps.

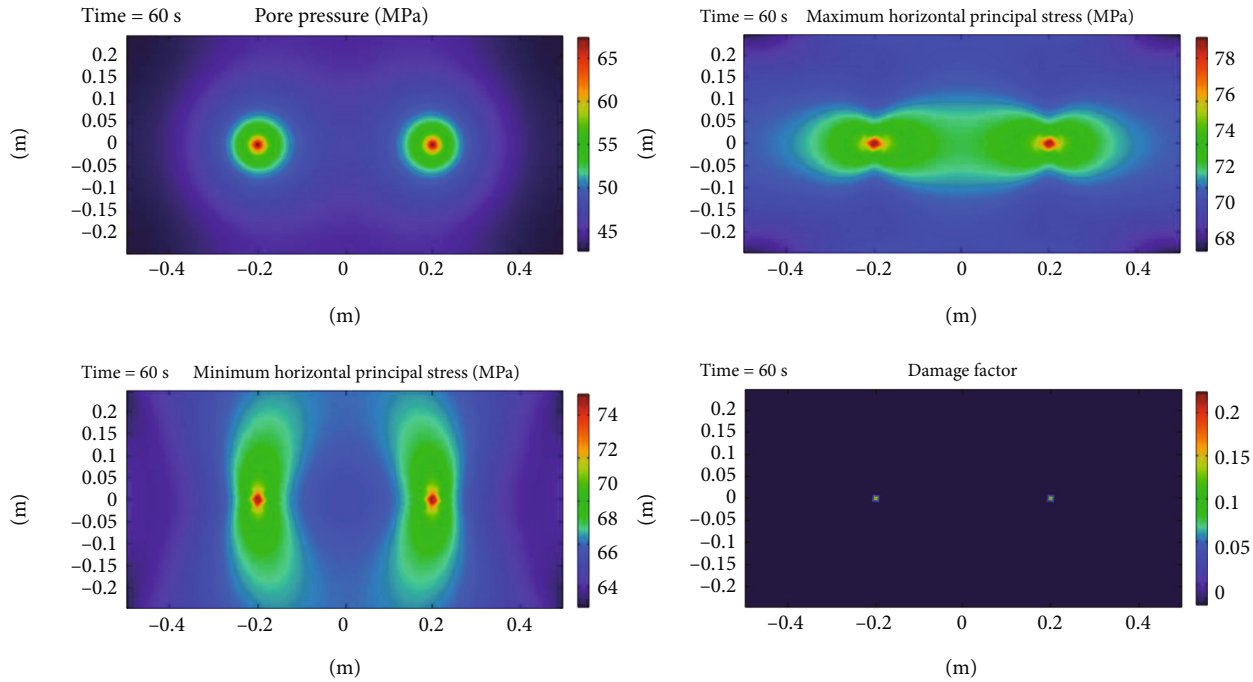

Figure 8: The distribution of pore pressure, the maximum horizontal principal stress, the minimum horizontal principal stress, and the damage factor in the two-perforation scenario at the last time step.

the base case. Then, the near-well damage caused by fluid injection operations from two perforations and three perforations with the same overall injection rate is discussed.

The two-perforation scenario is discussed first. In Figure 8, the distributions of pore pressure, the maximum horizontal principal stress, the minimum horizontal principal stress, and the damage factor at the final time step are presented. Note that the geometry of the domain is enlarged in the x direction to accommodate another perforation. Based on the 2D results, it can be noted that due to the increase in perforation number, the changes in pressure and stress are not as great as those in Figures 2–5. This is mainly caused by the decreased fluid injection rate in each perforation. A boundary effect on the distribution of the minimum horizontal principal stress can be found as well. Similar to the trends in Figures 3 and 4, the change in the minimum horizontal principal stress is greater in the direction of the initial $S_{h\ \min}$, and the change in the maximum horizontal principal stress is greater in the direction of the initial $S_{H\ \max}$. The magnitude and scale of damage in the

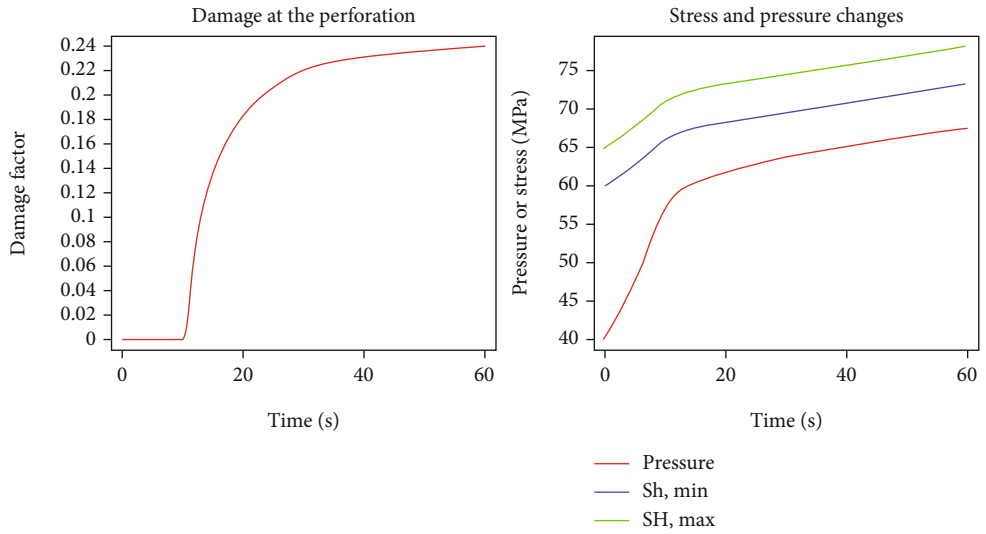

Figure 9: Damage, stress, and pressure evolutions at the perforation in the two-perforation scenario.

two-perforation case are insignificant compared to the single-perforation scenario, which is also related to the decreased fluid injection rate in each individual perforation.

The temporal evolution of pressure, stress, and damage at the perforation is also plotted in Figure 9. Due to symmetry, only the perforation on the left is discussed. Based on the curve for damage factor, fluid injection does not lead to damage right after the beginning of injection. As pore pressure is increased to a certain magnitude, the poroelastic behavior in the reservoir rock starts to cause damage. When the perforation number is increased to two, the pressure at the perforation cannot exceed the two horizontal principal stresses during the 60-second injection. This is also caused by the decreased injection rate per perforation. The pressure and stress curves indicate that, although the principal stress values are not surpassed by pore pressure values, damage can be initiated. However, due to the decreased injection rate, the damage factor profile in this scenario is largely lower than the damage factor profile in the base case where the injection rate per perforation is doubled. This is also reflected in the damage distribution result in Figure 8. Additionally, the stress curves are monotonically increasing in this scenario, and there are no oscillations, which is explained by the fact that a decreased injection rate per perforation avoids complicated effective stress evolutions from compressive states to tensile states in the rock skeleton.

Then, a three-perforation scenario is also presented to show and further present the effect of perforation number on the near-well damage. Since the overall injection rate is kept the same in the sensitivity analysis, the fluid injection rate per perforation is the lowest in the three-perforation scenario. In order to present the changes in variables related to near-well damage, the temporal evolution of pressure, stress, and damage is plotted in Figure 10. It is noticeable that there is no damage caused by fluid injection in the first 60 seconds. This exhibits that the further decreased fluid injection rate per perforation finally makes it impossible to initiate damage in 60 seconds. Note that only 60 seconds

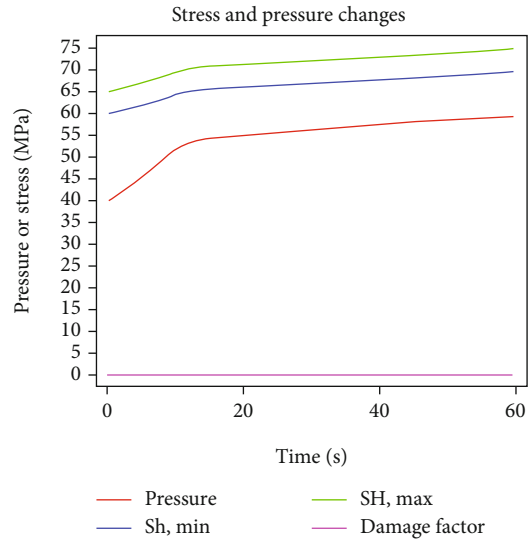

Figure 10: Damage, stress, and pressure evolutions at the perforation in the three-perforation scenario.

are investigated in this analysis and prolonged fluid injection further can still lead to near-well damage if the pore pressure is elevated enough. The increases in stress and pore pressure in 60 seconds are the lowest in the three perforation number scenarios, as the injection rate is distributed to three perforations.

The sensitivity analysis for perforation number indicates that more perforations during the fluid injection can decrease the ability to create injection-induced near-well damage, as the initiation and propagation of near-well damage are highly sensitive to the injection rate in each perforation. Therefore, during the hydraulic fracturing operation, it is important to guarantee the fluid injection rate distributed to individual perforations to enable the operations to create effective near-well damage, which is key to the initiation and propagation of hydraulic fractures.

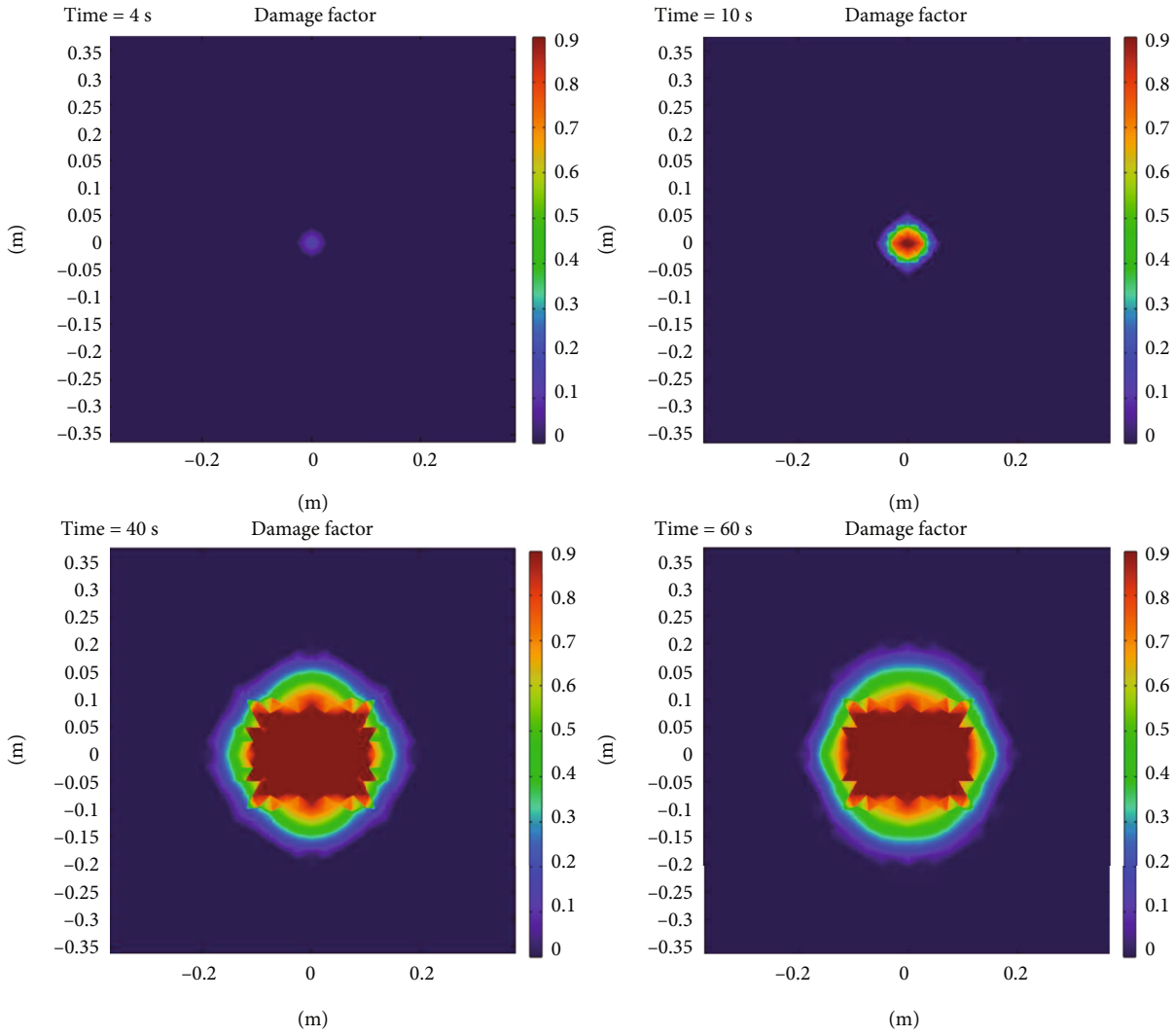

Figure 11: Damage distribution around the perforation after 4, 10, 40, and 60 seconds of injection with a rate of 0.075 kg/s.

3.4. Effects of Injection Rate. In the previous sensitivity analysis of the effect of perforation number on near-well damage, it is already concluded that the fluid injection rate distributed to each individual perforation is critical. Therefore, another analysis is carried out to examine the effect of injection rate on near-well damage. Note that the equivalent decreased injection rate in perforations is discussed in the previous section, and only magnified injection rates are investigated compared to the base case. Except for the base case injection rate of 0.05 kg/s, another two rates of 0.075 kg/s and 0.10 kg/s are analyzed. There is only one perforation in this part of the investigation.

Figure 11 shows the evolution of near-well damage around the perforation during the first 60 seconds of injection with a constant rate of 0.075 kg/s. The injection time steps shown are 4, 10, 40, and 60 seconds. The reason to show the damage on the fourth second is that it is the first time step with observed near-well damage. Compared to the base case, a 50% increase in the injection rate effectively magnifies the near-well damage scale. Also, the damaged region evolves faster. After 60 seconds of injection, the near-well damage can move to about 5 cm away from the perforation in the base case. In contrast, the near-well damage can move to 20 cm away from the perforation in the 0.075 kg/s injection scenario. Again, the damage travels further in the direction of the initial maximum horizontal principal stress. The damage factor can reach one in this scenario, meaning that the skeleton is completely damaged and hydraulic fractures can be initiated.

In Figure 12, the distribution of damage factor in the x and in the y directions is plotted at various time steps. It shows that an increased injection rate largely expedites the propagation of damage from the perforation. Compared to 5 cm propagation in 60 seconds in the base case, a constant injection rate of 0.075 kg/s can increase the damage propagation to about 20 cm away from the perforation. In the last 20 seconds, it is noted that the damage propagation does not travel as fast as in the first 40 seconds, indicating that the near-well damage propagation is more significant in the early stages. The transition of the damage factor is from totally damaged ($d = 1$) to undamaged ($d = 0$). Also, the damage distribution curves away from the perforation are

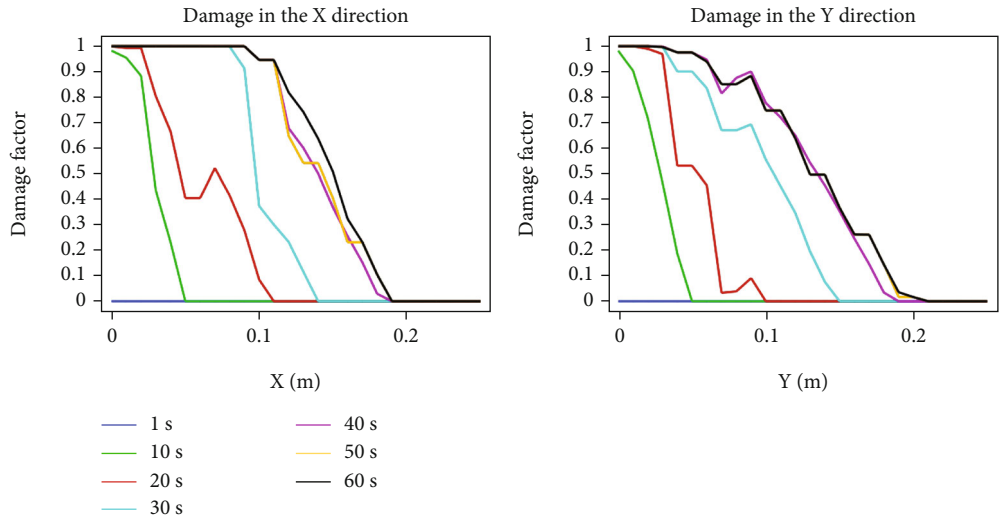

Figure 12: Damage distribution in the x and in the y directions at different time steps with an injection rate of 0.075 kg/s.

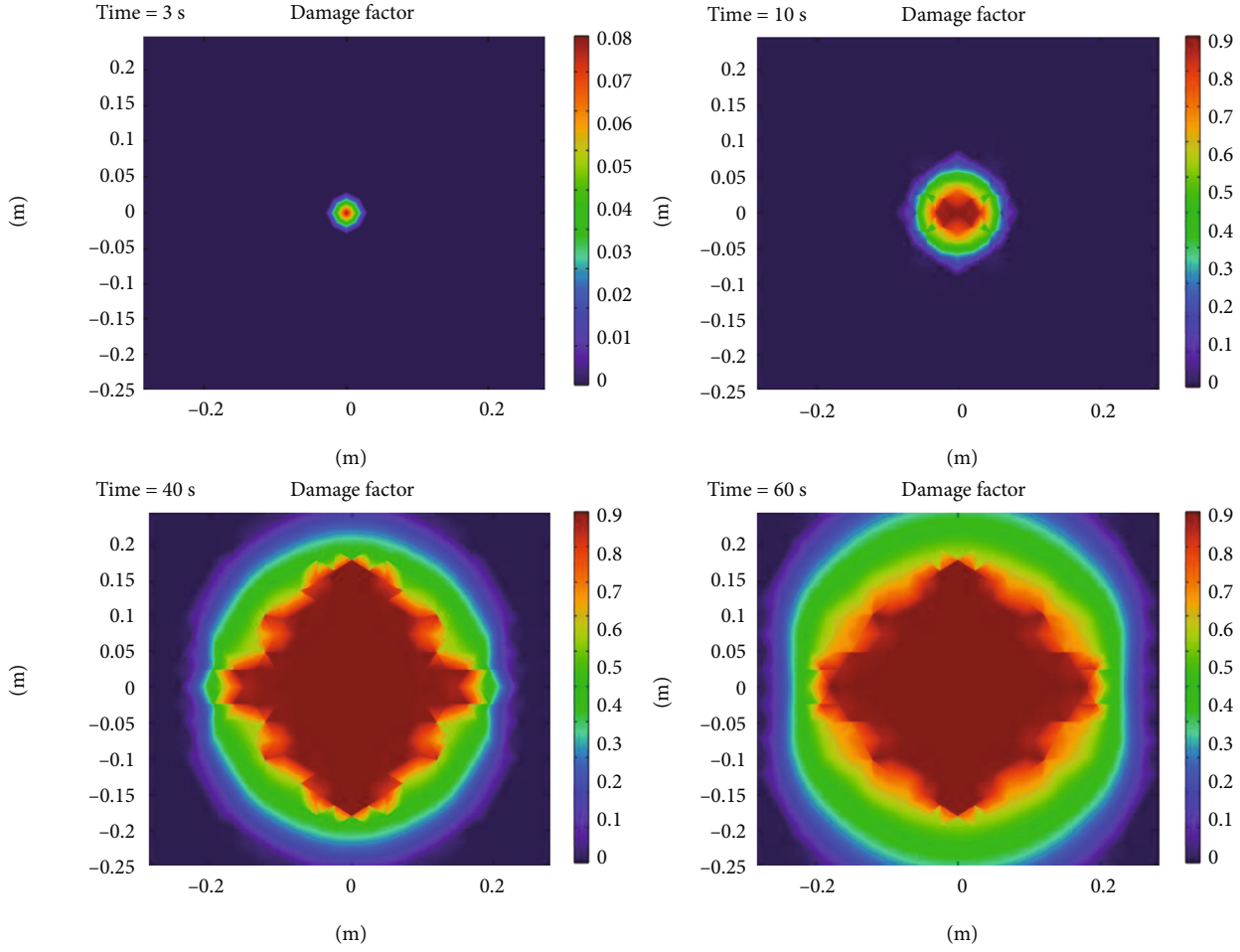

Figure 13: Damage distribution around the perforation after 3, 10, 40, and 60 seconds of injection with a rate of 0.10 kg/s.

oscillatory as the induced stress and strain changes are complicated and not monotonical. Meshing with unstructured grids leads to some fluctuations in the curves.

Then, the scenario with a constant injection rate of 0.10 kg/s is studied. The 2D damage distribution is presented in Figure 13. An increased injection rate can effectively

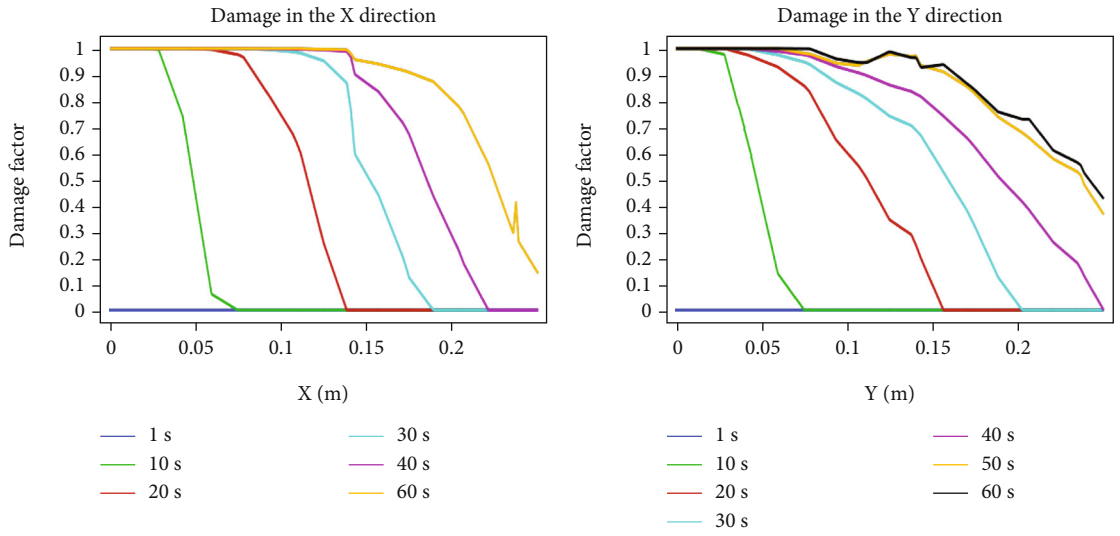

Figure 14: Damage distribution in the x and in the y directions at different time steps with an injection rate of 0.10 kg/s.

induce damage in the investigated domain, and the damage in this scenario is more extensive compared to the base case and the 0.075 kg/s injection rate case. The damage factor distribution on the third second is presented as it is the first time step with observed damage. Compared to Figure 12 where the first step with damage is the fourth second, an injection rate of 0.10 kg/s expedites the emergence of damage. It means that increasing the injection rate magnifies the evolving process of damage in the near-well region. In Figure 14, the distribution of damage in the x and y directions is plotted. Compared to the previous two scenarios with lower injection rates, this scenario has higher damage factor distribution profiles around the perforation. The entire 1D domain experiences damage, and the damage factors decrease as it moves away from the perforation. The magnitude of damage is the greatest among the three sensitivity scenarios.

Results in this study are focused on the initial stages during the fluid injection in a hydraulic fracturing operation. When the overall injection rate is kept constant, increasing perforation numbers leads to decreased efficiencies in achieving near-well damage, which can negatively affect the fracturing efficiency. In addition, before the initiation and propagation of the main fracture, areas experiencing near-well damage are limited, and continued fluid injection becomes less effective in obtaining new damaged areas after 40 seconds in this study. Therefore, perforation number and injection rate both affect the fracture initiation process. In hydraulic fracturing designing, less perforations and high injection rates help to obtain damage before the initiation and propagation of the main fracture.

4. Conclusions

In this study, a coupled hydromechanical model for the modeling of near-well damage evolution is presented. A case study is then carried out based on published datasets for the development of a shale oil reservoir in northwestern China. The effects of fluid injection time, perforation number, and fluid injection rate per perforation on the temporal and spatial evolution of near-well damage are investigated. In conclusion,

(1) Near-well damage evolves with time, and the movement of the damage front is faster in early stages and relatively slower in late stages. It indicates that there are limitations on the ultimate scale of damage propagation

(2) The damage factors in the direction of the initial maximum horizontal principal stress are greater than those in the direction of the initial minimum principal horizontal stress. This is in accordance with the fact in the hydraulic fracturing community that damage/fracture propagates in the direction of $S_{H\,\max}$

(3) The evolution of near-well damage is highly sensitive to the fluid injection rate. A decrease in the injection rate per perforation can largely reduce the scale and the magnitude of near-well damage and vice versa

(4) Based on the quantitative analysis in this numerical study, when the injection rate is constant, increasing the perforation number from one to two and three leads to decreases in the magnitudes of damage; the maximum damage factor decreases from 0.8 to 0.24 when the perforation number increases to two, while there is no damage factor observed when the perforation number is increased to three. When the injection rate is increased from 0.05 kg/s to 0.075 kg/s, the damaged radius increases from 0.05 m to 0.20 m; when the injection rate further increases to 0.10 kg/s, the damage radius can reach 0.3 m

Data Availability

Data are generated from the partial differential equation interface in the commercial software COMSOL Multiphysics. Access to the software can be obtained by purchasing a license.

Conflicts of Interest

The authors declare that they have no conflicts of interest.

Acknowledgments

The authors acknowledge financial support from the National Natural Science Foundation of China (nos. 51904314, 51991362, and U19B6003-05). The research is also sponsored by the CNPC Innovation Fund (no. 2021DQ02-0502), the Open Fund of the State Key Laboratory of Shale Oil and Gas Enrichment Mechanisms and Effective Development (no. 21-GJ-KF-16), and the China National Petroleum Corporation Major Science and Technology Project (nos. 2019E-26 and 2020F-50).

References

[1] M. Economides, A. D. Hill, C. Ehlig-Economides, and D. Zhu, *Petroleum Production Systems*, Pearson, 2013.

[2] Y. He, Y. Qiao, J. Qin, Y. Tang, Y. Wang, and Z. Chai, "A novel method to enhance oil recovery by inter-fracture injection and production through the same multi-fractured horizontal well," *Journal of Energy Resources Technology*, vol. 144, no. 4, article 043005, 2022.

[3] B. Hou, Z. Chang, W. Fu, Y. Muhadasi, and M. Chen, "Fracture initiation and propagation in a deep shale gas reservoir subject to an alternating-fluid-injection hydraulic-fracturing treatment," *SPE Journal*, vol. 24, no. 4, pp. 1839–1855, 2019.

[4] M. Marongiu-Porcu, M. J. Economides, and S. A. Holditch, "Economic and physical optimization of hydraulic fracturing," *Journal of Natural Gas Science and Engineering*, vol. 14, pp. 91–107, 2013.

[5] P. Tan, Y. Jin, L. Yuan et al., "Understanding hydraulic fracture propagation behavior in tight sandstone–coal interbedded formations: an experimental investigation," *Petroleum Science*, vol. 16, no. 1, pp. 148–160, 2019.

[6] N. Wijaya and J. J. Sheng, "Comparative study of well soaking timing (pre vs. post flowback) for water blockage removal from matrix-fracture interface," *Petroleum*, vol. 6, no. 3, pp. 286–292, 2020.

[7] X. Guo, Y. Jin, J. Zi, and B. Lin, "Numerical investigation of the gas production efficiency and induced geomechanical responses in marine methane hydrate-bearing sediments exploited by depressurization through hydraulic fractures," *Energy & Fuels*, vol. 35, no. 22, pp. 18441–18458, 2021.

[8] K. Nandlal and R. Weijermars, "Drained rock volume around hydraulic fractures in porous media: planar fractures versus fractal networks," *Petroleum Science*, vol. 16, no. 5, pp. 1064–1085, 2019.

[9] V. N. Nikolaevskiy and M. J. Economides, "The near-well state of stress and induced rock damage," in *SPE International Symposium on Formation Damage Control*, p. 58716, Lafayette, Louisiana, 2000.

[10] A. Settari and M. P. Cleary, "Development and testing of a pseudo-three-dimensional model of hydraulic fracture geometry," *SPE Production Engineering*, vol. 1, no. 6, pp. 449–466, 1986.

[11] Z. Cong, Y. Li, J. Tang, D. A. Martyushev, Hubuqin, and F. Yang, "Numerical simulation of hydraulic fracture height layer-through propagation based on three-dimensional lattice method," *Engineering Fracture Mechanics*, vol. 264, article 108331, 2022.

[12] W. L. Ellsworth, "Injection-induced earthquakes," *Science*, vol. 341, no. 6142, article 1225942, 2013.

[13] D. S. Cao, L. B. Zeng, W. Y. Lü, X. Xu, and H. Tian, "Progress in brittleness evaluation and prediction methods in unconventional reservoirs," *Petroleum Science Bulletin*, vol. 6, no. 1, pp. 31–45, 2021.

[14] M. W. McClure and R. N. Horne, "An investigation of stimulation mechanisms in enhanced geothermal systems," *International Journal of Rock Mechanics and Mining Sciences*, vol. 72, pp. 242–260, 2014.

[15] J. J. Zhang, *Applied Petroleum Geomechanics*, Gulf Professional Publishing, 2020.

[16] H. Y. Zhu, X. C. Jin, J. C. Guo, F. C. An, Y. H. Wang, and X. D. Lai, "Coupled flow, stress and damage modelling of interactions between hydraulic fractures and natural fractures in shale gas reservoirs," *International Journal Of Oil Gas And Coal Technology*, vol. 13, no. 4, pp. 359–390, 2016.

[17] S. M. Patel, C. H. Sondergeld, and C. S. Rai, "Laboratory studies of hydraulic fracturing by cyclic injection," *International Journal of Rock Mechanics and Mining Sciences*, vol. 95, pp. 8–15, 2017.

[18] L. Huang, P. Jiang, X. Zhao, L. Yang, J. Lin, and X. Guo, "A modeling study of the productivity of horizontal wells in hydrocarbon-bearing reservoirs: effects of fracturing interference," *Geofluids*, vol. 2021, Article ID 2168622, 13 pages, 2021.

[19] X. Shi, Y. Qin, H. Xu et al., "Numerical simulation of hydraulic fracture propagation in conglomerate reservoirs," *Engineering Fracture Mechanics*, vol. 248, article 107738, 2021.

[20] R. W. Zimmerman and G. S. Bodvarsson, "Hydraulic conductivity of rock fractures," *Transport in Porous Media*, vol. 23, no. 1, pp. 1–30, 1996.

[21] X. Guo, K. Wu, C. An, J. Tang, and J. Killough, "Numerical investigation of effects of subsequent parent-well injection on interwell fracturing interference using reservoir-geomechanics-fracturing modeling," *SPE Journal*, vol. 24, no. 4, pp. 1884–1902, 2019.

[22] N. Roussel and M. Sharma, "Strategies to Minimize Frac Spacing and Stimulate Natural Fractures in Horizontal Completions," in *SPE annual technical conference and exhibition*, Denver, Colorado, USA, 2011.

[23] A. Chen, X. Guo, H. Yu, L. Huang, S. Shi, and N. Cheng, "A parametric study of hydraulic fracturing interference between fracture clusters and stages based on numerical modeling," *Energy Exploration & Exploitation*, vol. 39, no. 1, pp. 65–85, 2021.

[24] G. Fowler, D. Ratcliff, and M. McClure, "Modeling frac hits: mechanisms for damage versus uplift," in *Paper presented at the International Petroleum Technology Conference*, Riyadh, Saudi Arabia, February 2022.

[25] N. P. Roussel, H. A. Florez, and A. A. Rodriguez, "Hydraulic fracture propagation from infill horizontal wells," in *SPE*

Annual Technical Conference and Exhibition, New Orleans, Louisiana, USA, 2013.

[26] C. Shi and B. Lin, "Principles and influencing factors for shale formations," *Petroleum Science Bulletin*, vol. 1, pp. 92–113, 2021.

[27] A. Hardcastle, M. M. Nezhad, M. Rezania, W. Tizani, and P. G. Ranjith, "A fully coupled computational framework for fluid pressurized crack evolution in porous media," *Journal of Porous Media*, vol. 22, no. 8, pp. 939–956, 2019.

[28] Q. Lei, N. G. Doonechaly, and C. F. Tsang, "Modelling fluid injection-induced fracture activation, damage growth, seismicity occurrence and connectivity change in naturally fractured rocks," *International Journal of Rock Mechanics and Mining Sciences*, vol. 138, article 104598, 2021.

[29] K. F. Evans, A. Genter, and J. Sausse, "Permeability creation and damage due to massive fluid injections into granite at 3.5 km at Soultz: 1. Borehole observations," *Journal of Geophysical Research - Solid Earth*, vol. 110, no. B4, pp. 1–19, 2005.

[30] X. Wang, L. Liang, L. Zhao, X. Liu, Z. Qin, and W. Li, "Rock mechanics and fracability evaluation of the Lucaogou formation oil shales in Jimusaer sag, Junggar Basin," *Oil & Gas Geology*, vol. 40, no. 3, pp. 661–668, 2019.

[31] Z. Wang, X. Guo, G. Zheng et al., "Effects of parent well spacing on the poroelastic behaviors in the infill zone in shale oil reservoirs: a case study in Jimsar Shale Oil, China," *Energy Science & Engineering*, vol. 10, no. 4, pp. 1043–1054, 2022.

[32] D. Zhi, X. Guo, W. Wang et al., "Fracturing and production analysis of the efficacy of hydraulic fracture stage reduction in the improvement of cost-effectiveness in shale oil development: a case study of Jimsar shale oil, China," *Energy Science & Engineering*, vol. 9, no. 9, pp. 1337–1348, 2021.